Vol. 92 No. 2 pp. 586–599 ACTA GEOLOGICA SINICA (English Edition) Apr. 2018

Exsolution Lamellae in Olivine Grains of Dunite Units from Different Types of Mafic-Ultramafic Complexes

LIANG Zi[1, 2, *], XIAO Yan[1, *], Joyashish THAKURTA[3], SU Benxun[2, 4], CHEN Chen[2, 4], BAI Yang[2, 4] and Patrick A. SAKYI[5]

1 *State Key Laboratory of Lithospheric Evolution, Institute of Geology and Geophysics, Chinese Academy of Sciences, Beijing 100029, China*

2 *University of Chinese Academy of Sciences, Beijing 100049, China*

3 *Department of Geosciences, Western Michigan University, 1903 West Michigan Avenue, Kalamazoo, MI 49008, USA*

4 *Key Laboratory of Mineral Resources, Institute of Geology and Geophysics, Chinese Academy of Sciences, Beijing 100029, China*

5 *Department of Earth Science, School of Physical and Mathematical Sciences, University of Ghana, Legon-Accra, Ghana*

Abstract: Exsolution microstructures in olivine grains from dunite units in a few selected tectonic environments are reported here. They include lamellae of clinopyroxene and clinopyroxene-magnetite intergrowth in the Gaositai and Yellow Hill Alaskan-type complexes, clinopyroxene-magnetite intergrowth in the Kızıldağ ophiolite, and chromite lamellae in the Hongshishan mafic-ultramafic intrusive complex. These lamellae commonly occur as needle- or rod-like features and are oriented in olivine grains. The host olivine grains have Fo contents of 92.5–92.6 in the Gaositai complex, 86.5–90.1 in the Yellow Hill complex, 93.2–93.4 in the Kızıldağ ophiolite and 86.9–88.3 in the Hongshishan complex. Clinopyroxene in the rod-like intergrowth exsolved in olivine grains in the Gaositai and Yellow Hill is diopside with similar major element compositions of CaO (23.6–24.3wt%), SiO_2 (52.2–54.0wt%), Al_2O_3 (0.67–2.15wt%), Cr_2O_3 (0.10–0.42wt%) and Na_2O (0.14–0.26wt%). It falls into the compositional field of hydrothermal clinopyroxene and its origin is thus probably related to reaction between dunite and fluids. The enrichment of the fluids in Ca^{2+}, Fe^{3+}, Cr^{3+} and Na^{+}, resulted in elevated concentrations of these cations in olivine solid solutions via the reaction. With decreasing temperature, the olivine solid solutions altered to an intergrowth of magnetite and clinopyroxene. The Fe^{3+} and Cr^{3+} preferentially partitioned into magnetite, while Ca^{2+} and Na^{+} entered clinopyroxene. Since the studied Alaskan-type complexes and ophiolite formed in a subduction environment, the fluids were probably released from the subducted slab. In contrast, the exsolved chromite in olivine grains from the Hongshishan complex that formed in post-orogenic extension setting can be related to olivine equilibrated with Cr-bearing liquid. Similarly, these lamellae have all been observed in serpentine surrounding olivine grains, indicating genetic relations with serpentinization.

Key words: olivine, dunite, clinopyroxene lamella, intergrowth of clinopyroxene and magnetite, mafic-ultramafic complex

1 Introduction

Exsolution is a process in which an initially homogeneous solid solution turns metastable, and subsequently separates into at least two self-equilibrated phases (Colás et al., 2016). This process is associated with the changes of physicochemical conditions such as temperature, pressure and oxygen fugacity. Thus, studies on chemical compositions of submicrometer-sized thin lamellae and their relationship with host mineral are important for understanding physicochemical conditions of the homogeneous precursor, geochemical cycling and

* Corresponding author. E-mail: liangzi@mail.iggcas.ac.cn (Z. Liang) and xiaoyan@mail.iggcas.ac.cn (Y. Xiao)

mantle dynamics (e.g., Zhang et al., 1999, 2017). The exsolution microstructures are wide-spread in clinopyroxene of mafic-ultramafic rocks because clinopyroxene can accommodate large cations. Exsolution of garnet in clinopyroxene has been widely reported in clinopyroxene megacrysts (Aoki et al., 1980) and eclogite (Green, 1966; Jerde et al., 1993; Zhang and Liou, 2003; Schmickler et al., 2004). Such exsolution phenomena were generally attributed to changes of thermal conditions (Aoki et al., 1980; Sautter and Hart, 1988, 1990; Jerde et al., 1993; Zhang and Liou, 2003). Exsolution of K-feldspar (Zhu, 2003) and phlogopite-coesite intergrowth (Zhu and Ogasawara, 2002) were observed in clinopyroxene in peridotite (Zhao Wenxia et al., 2004; Bozhilov et al., 1999). Coesite and clinopyroxene exsolution in chromite was also reported in podiform chromitite of the Luobusa ophiolite, Tibet, which was explained by pressure change from 12.5 GPa to 3 GPa (Yamamoto et al., 2009).

Olivine is simple in structure and composition, has small radii of the M1 and M2 cationic sites, and thus rarely forms exsolution lamellae. However, olivine grains with various kinds of exsolved lamellae such as ilmenite, chromite, magnetite, and intergrowth of clinopyroxene and magnetite have been reported in meteorite, alpine peridotite, layered intrusion and ophiolite (Arai, 1978; Ashworth, 1979; Moseley, 1981; Green and Gueguen, 1983; Drury and Van Roermund, 1988; Mikouchi et al., 1995; Zhang et al., 1999; Ren Yufeng et al., 2008; Xiong Fahui et al., 2015, 2016; Xiong et al., 2017). Although changes in physical conditions, such as temperature, pressure and oxygen fugacity, have been known to cause exsolution lamellae, the chemical origin of some elements which are rare in olivine remains uncertain.

In this study, we report occurrences of clinopyroxene lamellae and clinopyroxene-magnetite intergrowth in olivine grains from dunite units in the Gaositai Alaskan-type complex, northern part of the North China Craton and Yellow Hill Alaskan-type complex, southeastern Alaska, clinopyroxene-magnetite intergrowth in the Kızıldağ ophiolite, southeastern Turkey, as well as chromite lamellae in the Hongshishan mafic-ultramafic complex, Central Asian Orogenic Belt. These new findings of exsolution microstructures, together with chemical compositions of olivine grains, have been used to constrain the mechanism of exsolution in olivine.

2 Geology of Studied Mafic-ultramafic Complexes

2.1 Gaositai Alaskan-type complex

The Gaositai complex is located in the northern margin of the North China Craton (Chen et al., 2009; Fig. 1). It is concentrically zoned with dunite in the core, rimmed by successive wehrlite, clinopyroxenite and hornblendite, which is typical of Alaskan-type complex (Chen et al., 2009; Tian et al., 2011). The central dunite body is the largest lithological unit in the complex, and is composed mainly of olivine and minor chromite. Olivine crystals are commonly replaced by serpentine (Fig. 2a–c).

2.2 Yellow Hill Alaskan-type complex

The Yellow Hill Alaskan-type complex is located in Annette Island, southern end of Alaskan panhandle, in the United States of America (Gehrels et al., 1987; Li et al., 2013; Fig. 1), and is mainly composed of dunite with minor wehrlite (Gehrels et al., 1987). The dunite consists of olivine, minor chromite and interstitial clinopyroxene. Olivine grains show variable degrees of serpentinization (Fig. 2d–f).

2.3 Kızıldağ ophiolite

The Kızıldağ ophiolite is located in southern Turkey (Fig. 1) and has been interpreted as a remnant of a regional -scale slice of oceanic lithosphere (Hall, 1976; Boulton and Robertson, 2007; Dilek and Thy, 2009; Dilek and Furnes, 2017). It constitutes a complete ophiolitic sequence of mantle tectonite, ultramafic to mafic cumulate, isotropic gabbro, sheeted dike, plagiogranite and volcanic complex. The dunite occurs as lenticular layers surrounded by harzburgite. It is composed of olivine with minor chromite exhibiting cumulus textures (Chen et al., 2015).

2.4 Hongshishan mafic-ultramafic complex

The Hongshishan mafic-ultramafic complex is an intrusion situated in the southern margin of the Central Asian Orogenic Belt (Fig. 1). It consists of ultramafic units such as dunite, wehrlite and troctolite, and a mafic unit of gabbro and minor diorite (Su Benxun et al., 2009; Su et al., 2012). The dunite is located in the center of the intrusion and has an inferred thickness of 230 m based on drilling records. It is characterized by cumulus texture and contains olivine (>90 vol.%) with variable amounts of chromite, clinopyroxene and plagioclase (Su Benxun et al., 2009).

3 Analytical Methods

3.1 Major element analysis of minerals

Major element compositions of minerals in the dunite from the Gaositai complex, Kızıldağ ophiolite and Hongshishan mafic-ultramafic complex were determined by wavelength-dispersive X-ray spectrometry with a JEOL

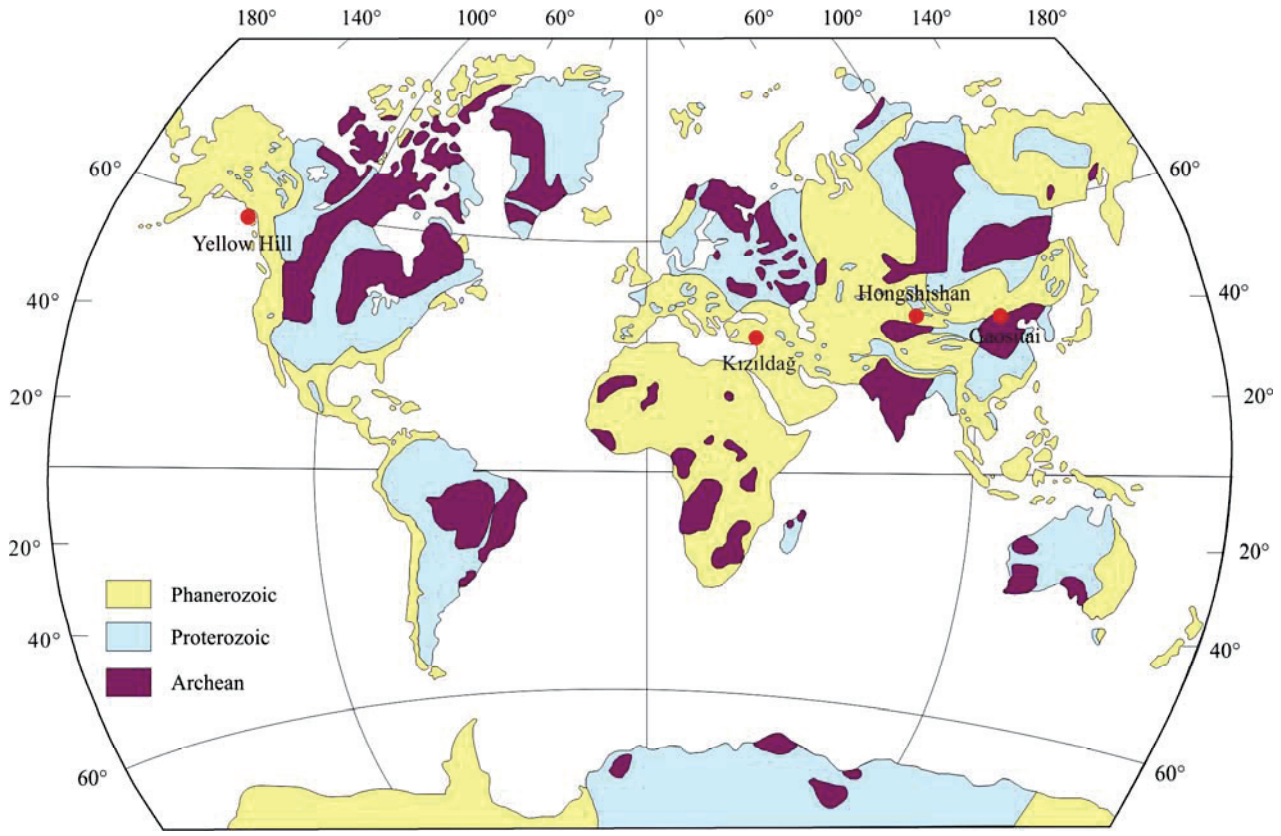

Fig. 1. Spatial distribution of the Gaositai and Yellow Hill Alaskan-type complexes, Kızıldağ ophiolite and Hongshishan complex (modified from Kerrich and Polat 2006).

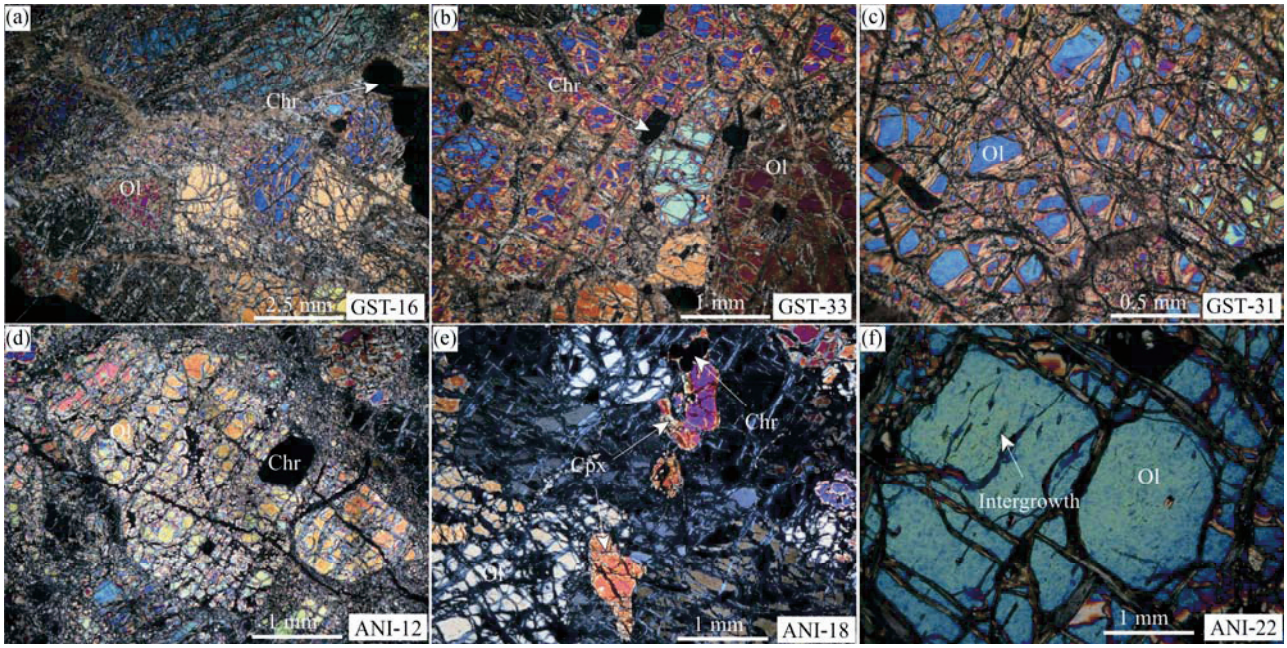

Fig. 2. Photomicrographs of dunite samples in the Gaositai (a–c) and Yellow Hill complexes (d–f).

JXA8100 electron probe microanalyzer at the Institute of Geology and Geophysics, Chinese Academy of Sciences (IGGCAS). Major element compositions of minerals in the dunite from the Yellow Hill complex were obtained from wavelength-dispersive X-ray spectrometry with a JEOL JXA8230 electron probe microanalyzer at State Key Laboratory of Continental Dynamics in Northwest University. Both analyses were operated at an accelerating voltage of 15 kV and 10 nA beam current, 5 μm beam size and peak counting time of 10-30 s, whilst the analysis of

clinopyroxene in the exsolved rod intergrowth was carried out with a 1 μm beam size. Natural and synthetic standards were used during the analyses. Matrix effects were corrected by a program based on the ZAF procedure. Typical analytical uncertainty for the elements analyzed was better than 1.5%. Natural minerals such as jadeite [$NaAlSiO_6$] for Na, Al and Si, rhodonite [$MnSiO_3$] for Mn, sanidine [$KAlSi_3O_8$] for K, garnet [$Fe_3Al_2Si_3O_{12}$] for Fe, Cr-diopside [(Mg, Cr)$CaSi_2O_6$] for Ca, olivine [(Mg, Fe)$_2SiO_4$] for Mg and synthetic minerals (rutile for Ti, 99.7% Cr_2O_3 for Cr, Ni_2Si for Ni) were used for standard calibration, and a program based on the ZAF procedure was used for matrix corrections.

3.2 Elemental mapping and energy dispersive spectrometry

All the samples with polished sections were analyzed by SEM on a FEI NOVA nano450 scanning electron microscope equipped with energy dispersive spectrometry at IGGCAS. Backscattered electron images were obtained at 15 kV accelerating voltage and 3.5 nA beam current. The point analysis and mapping of energy dispersive spectrometry were obtained at the same conditions used for the acquisition of the backscattered electron images.

4 Structures and Chemical Compositions of Exsolution and Host Olivine

4.1 Gaositai Alaskan-type complex

The exsolution of clinopyroxene-magnetite intergrowth was observed in olivine grains of the Gaositai dunite (Fig. 3a–d). It is oriented and confined within the interior of the host olivine grains (Fig. 3a–d). The intergrowth is normally 0.05 to 10 μm in width and 5 to >30 μm in length. These intergrowths are dominated by needle-like intergrowths of clinopyroxene and magnetite, where clinopyroxene usually grows in between two magnetite lamellae (Figs. 3–4). Rod-like intergrowths are parallel to needle-like intergrowths (Fig. 3a–c). In addition, rare clinopyroxene needles occur alone and always grow parallel to the exsolved intergrowth (Fig. 3d).

The rod-like clinopyroxenes exsolved in olivine grains are diopside with major element compositions of CaO (23.6–24.1wt%), SiO_2 (53.0–54.0wt%), Al_2O_3 (0.67–1.64wt%), Cr_2O_3 (0.10–0.32wt%) and Na_2O (0.18–0.26wt%) (Table 1). The host olivine grains in the Gaositai dunite have restricted MgO (49.5–51.8wt%), SiO_2 (40.5–42.6wt%) and CaO (0.14–0.24wt%) contents (Fig. 5a–b; Table 1). The lamella-free and lamella-bearing olivine grains in the Gaositai dunite have similar chemical compositions (Fig. 4). The $Mg^{\#}$ of rod-like clinopyroxene ranges from 92.5 to 94.1, which are similar to Fo (92.5) of the host olivine grains (Table 1).

The estimated temperatures using the olivine-spinel thermometer of Ballhaus et al. (1991) for dunites in the Gaositai complex range from 751 to 855°C (Table 2).

4.2 Yellow Hill Alaskan-type complex

Clinopyroxene lamellae and clinopyroxene-magnetite intergrowth are also present in the olivine grains of the

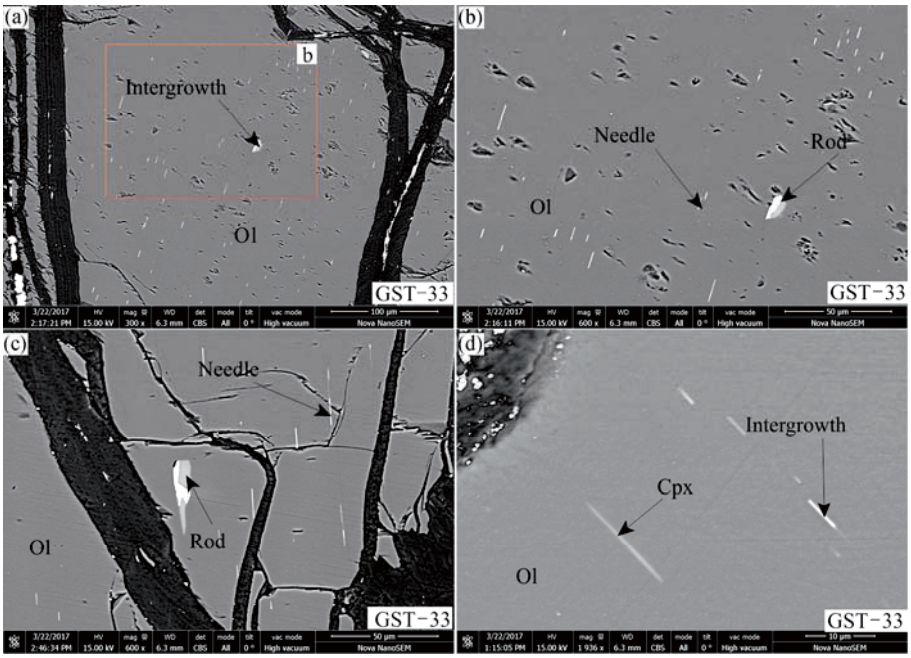

Fig. 3. Backscattered electron images of exsolved lamellae in olivine grains from the Gaositai dunite (a–d); Clinopyroxene-magnetite intergrowth in shape of needle and rod in host olivine grains (a–c); Clinopyroxene lamellae with coexisting needle-like intergrowths in host olivine grains (d). Ol, olivine, Cpx, clinopyroxene, Chr, chromite, Mag, magnetite.

Table 1 Major element compositions (wt%) of olivine and clinopyroxene in the dunite samples from the Gaositai and Yellow Hill Alaskan-type complexes, Kýzýldað ophiolite and Hongshishan complex

Sample	GST-13	GST-15	GST-17	GST-16	GST-31	GST-31	GST-21	GST-21	GST-18	GST-33	GST-33
Mineral	LFQ	LFQ	LFQ	LFQ	LFQ	LFQ	LFQ	LFQ	LFQ	LFQ	LFQ
SiO_2	41.9	41.5	41.7	41.7	42.3	42.0	42.6	42.0	41.2	41.5	41.1
TiO_2	0.01	0.01	0.01	0.01	0.01	0.01	0.01	0.00	0.01	0.02	0.02
Al_2O_3	0.00	0.00	0.00	0.00	0.00	0.00	0.00	0.00	0.00	0.00	0.00
Cr_2O_3	0.02	0.03	0.02	0.05	0.07	0.04	0.02	0.03	0.01	0.02	0.03
FeO	7.24	7.43	7.63	6.45	6.04	7.58	7.33	7.27	7.70	7.34	7.29
MnO	0.15	0.14	0.14	0.12	0.10	0.15	0.13	0.13	0.13	0.13	0.14
MgO	50.7	50.5	50.2	51.4	51.8	50.7	50.7	50.5	49.5	50.7	51.3
CaO	0.19	0.21	0.21	0.16	0.14	0.21	0.16	0.24	0.21	0.16	0.22
Na_2O	0.00	0.00	0.00	0.01	0.01	0.01	0.00	0.00	0.00	0.00	0.01
K_2O	0.01	0.00	0.00	0.00	0.01	0.00	0.01	0.00	0.01	0.01	0.01
NiO	0.25	0.26	0.25	0.24	0.24	0.26	0.24	0.26	0.25	0.26	0.25
Total	100	100	100	100	101	101	101	100	99.1	100	100
$Mg^{\#}$	92.7	92.4	92.2	93.4	93.9	92.3	92.6	92.6	92.1	92.6	92.7
Sample	GST-18	GST-18	GST-18	GST-33	GST-33	GST-33	YH-05	ANI-20	ANI-13	ANI-10	ANI-05
Mineral	LBQ	CR	CR	LBQ	CR	CR	LFQ	LFQ	LFQ	LBQ	LBQ
SiO_2	40.5	54.0	53.0	41.8	53.2	53.6	40.7	40.7	40.7	40.5	41.1
TiO_2	0.03	0.04	0.04	0.00	0.16	0.15	0.01	0.02	0.01	0.00	0.00
Al_2O_3	0.00	0.67	0.98	0.00	1.64	1.64	0.00	0.00	0.01	0.00	0.00
Cr_2O_3	0.03	0.10	0.23	0.03	0.29	0.32	0.02	0.02	0.02	0.00	0.04
FeO	7.43	2.10	2.62	7.39	2.70	2.75	10.2	9.56	11.0	13.0	9.72
MnO	0.15	0.00	0.04	0.14	0.05	0.04	0.16	0.16	0.16	0.18	0.16
MgO	50.6	18.6	18.7	50.6	18.0	17.9	48.2	49.0	47.9	46.6	49.1
CaO	0.19	24.1	23.6	0.17	23.8	23.8	0.16	0.15	0.17	0.12	0.10
Na_2O	0.01	0.22	0.26	0.00	0.18	0.18	0.00	0.01	0.00	0.01	0.01
K_2O	0.25	0.01	0.00	0.25	0.00	0.00	0.01	0.01	0.01	0.01	0.01
NiO	0.25	0.02	0.05	0.25	0.04	0.07	0.08	0.16	0.11	0.13	0.16
Total	99.4	99.8	99.5	101	100	100	99.6	99.9	100	101	100
$Mg^{\#}$	92.5	94.1	92.8	92.5	92.3	92.1	89.4	90.1	88.6	86.5	90.0
Sample	ANI-12	ANI-15	ANI-22	ANI-16	ANI-18	ANI-22	ANI-22	ANI-22	KZ14-28	KZ14-28	HS382	HS473
Mineral	LBQ	LBQ	LBQ	LBQ	LBQ	CR	CR	CR	OWL	LBQ	LBQ	LBQ
SiO_2	40.9	40.5	40.6	40.7	40.6	52.2	52.2	52.6	41.8	41.7	41.5	40.6
TiO_2	0.02	0.00	0.00	0.00	0.01	0.11	0.13	0.07	0.01	0.01	0.02	0.03
Al_2O_3	0.01	0.01	0.00	0.00	0.00	2.15	1.57	0.87	0.00	0.00	0.00	0.00
Cr_2O_3	0.01	0.01	0.01	0.01	0.01	0.39	0.42	0.18	0.03	0.01	0.02	0.01
FeO	10.0	11.1	10.7	9.90	10.0	4.06	3.56	4.00	6.63	6.56	12.6	11.4
MnO	0.12	0.14	0.18	0.13	0.18	0.03	0.03	0.04	0.09	0.10	0.20	0.18
MgO	49.0	47.5	47.9	48.6	48.4	16.9	17.3	17.7	50.5	51.2	46.5	47.6
CaO	0.03	0.07	0.06	0.02	0.03	24.1	24.1	24.3	0.20	0.21	0.05	0.06
Na_2O	0.01	0.00	0.00	0.00	0.00	0.21	0.15	0.14	0.01	0.00	0.00	0.00
K_2O	0.01	0.01	0.01	0.00	0.00	0.00	0.00	0.00	0.00	0.00	0.00	0.00
NiO	0.15	0.12	0.18	0.09	0.08	0.04	0.00	0.04	0.42	0.42	0.17	0.29
Total	100	99.5	99.7	99.6	99.4	100	99.4	100	99.7	100	101	100
$Mg^{\#}$	89.8	88.4	88.9	89.8	89.6	88.1	89.7	88.7	93.2	93.4	86.9	88.3

Note: LFQ: Lamella-free olivine; LBQ: Lamella-bearing olivine; CR: clinopyroxene rod in Ol; OWL: olivine without lamellae. $Mg^{\#}=100 \times Mg^{2+}/(Mg^{2+}+Fe^{2})$

Yellow Hill dunite. The intergrowth has lengths ranging from <5 to >20 μm and widths from 0.05 to >5 μm, and commonly occurs as oriented needles or rods (Figs. 6a–f, 7). Clinopyroxene lamellae confined in the core of olivine grains are commonly parallel to the exsolved intergrowth. The clinopyroxene lamellae and intergrowth show random orientations in the olivine grains. The olivine grains in the dunite unit of the Yellow Hill Complex show more clinopyroxene lamellae than those in the dunite of the Gaositai complex (Fig. 6c–f).

The clinopyroxene in the intergrowth rod exsolved in olivine grains of the Yellow Hill dunite has CaO (24.1–24.3wt%), Al_2O_3 (0.87–2.15wt%), SiO_2 (52.2–52.6wt%) and Cr_2O_3 (0.18–0.42wt%) contents similar to those in the Gaositai complex (Table 1). The exsolved magnetite in olivine grains shows lower Cr_2O_3 content (Fig. 7). The host olivine grains have lower MgO (46.6–49.0wt%) and CaO (0.02–0.17wt%), and higher FeO (9.56–13.0wt%) contents than those in the Gaositai dunite (Fig. 8a, b). The $Mg^{\#}$ of clinopyroxene rod varies from 88.1 to 89.7 and the host olivine has Fo of 88.9 (Table 1). The equilibrium temperature estimates vary from 659 to 773°C (Table 2).

4.3 Kızıldağ ophiolite

The intergrowth of clinopyroxene and magnetite in the studied dunite sample from the Kızıldağ ophiolite is 0.5 to 1 μm in length and 0.05 to 0.5 μm wide and occurs without a single clinopyroxene lamellae. They are needle-like or rod-like in shape and are aligned parallel to each other (Fig. 9a–d).

The olivine grains in the Kızıldağ dunite have homogeneous MgO (49.2–51.6wt %), CaO (0.04–

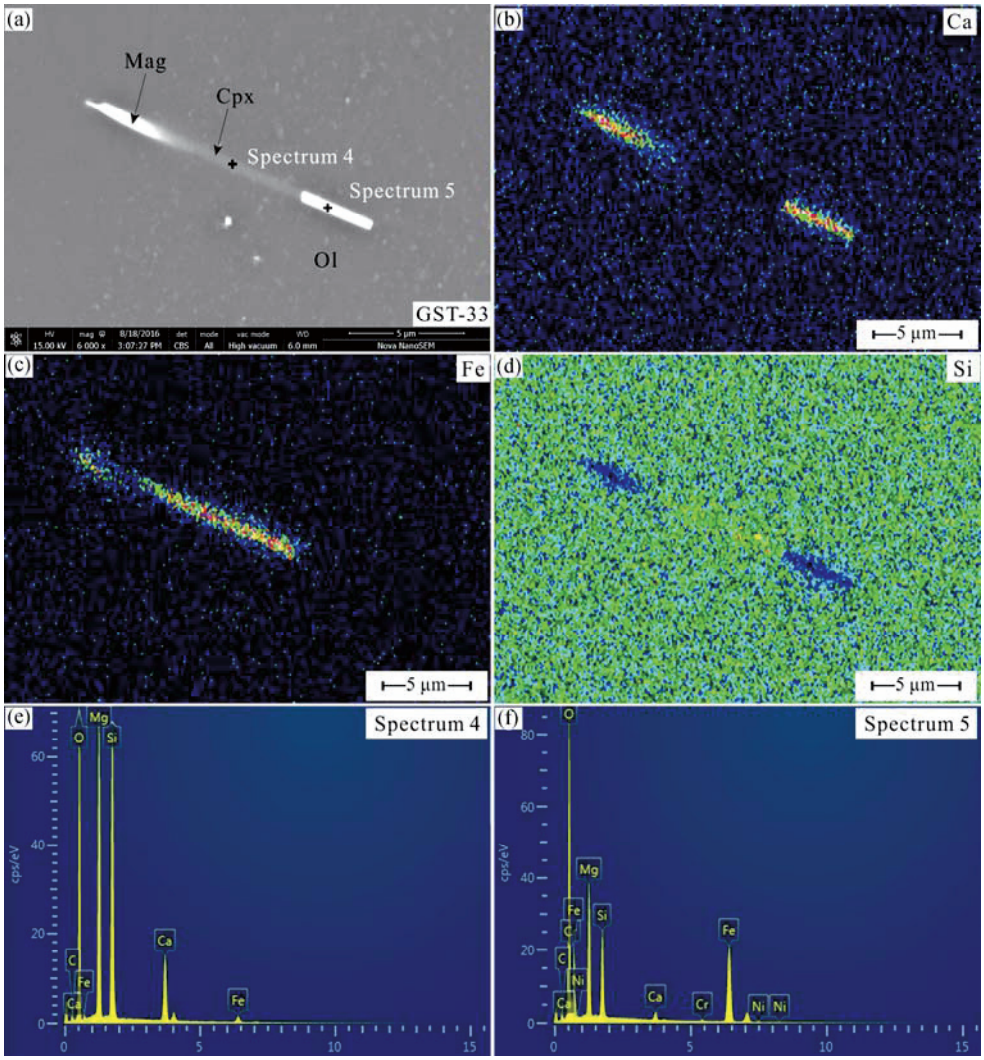

Fig. 4. Backscattered electron images of exsolved intergrowth in olivine grain of the Gaositai dunite (a); Elemental mapping (Ca, Fe and Si) of clinopyroxene lamellae and clinopyroxene-magnetite intergrowth in olivine from the Gaositai dunite (b–d); Energy dispersive spectrometry analysis of clinopyroxene-magnetite intergrowth (e–f).

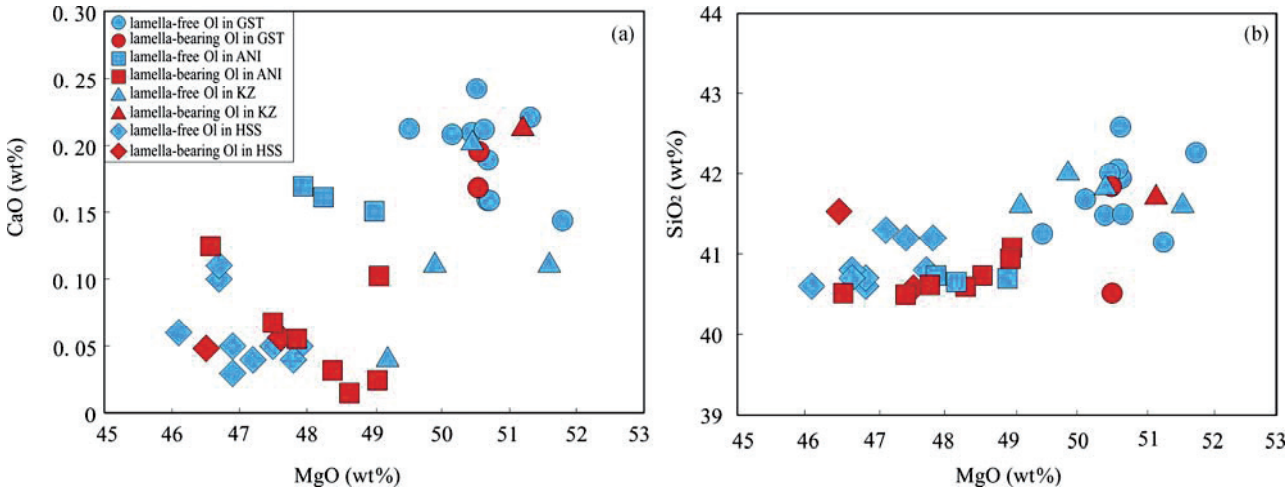

Fig. 5. Correlation diagrams of MgO with (a) CaO and (b) SiO_2 for lamella-bearing and lamella-free olivine grains in a dunite unit from the Gaositai and Yellow Hill Alaskan-type complexes, Kızıldağ ophiolite and Hongshishan complex.

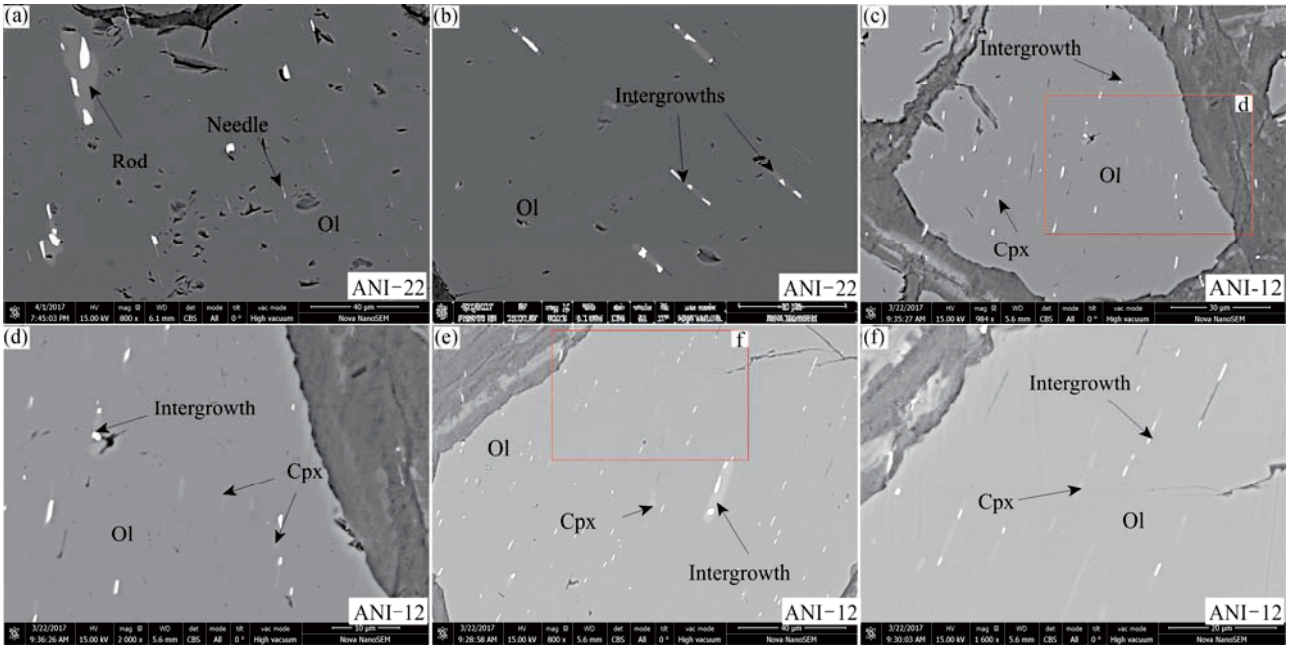

Fig. 6. Backscattered electron images of exsolved lamellae in olivine grains from the Yellow Hill dunite (a–f); Backscattered electron images of clinopyroxene-magnetite intergrowth in the shape of rod or needle (a–b); abundance of exsolved clinopyroxene with coexisting needle-like and rod-like intergrowths in host olivine grains (c–f).

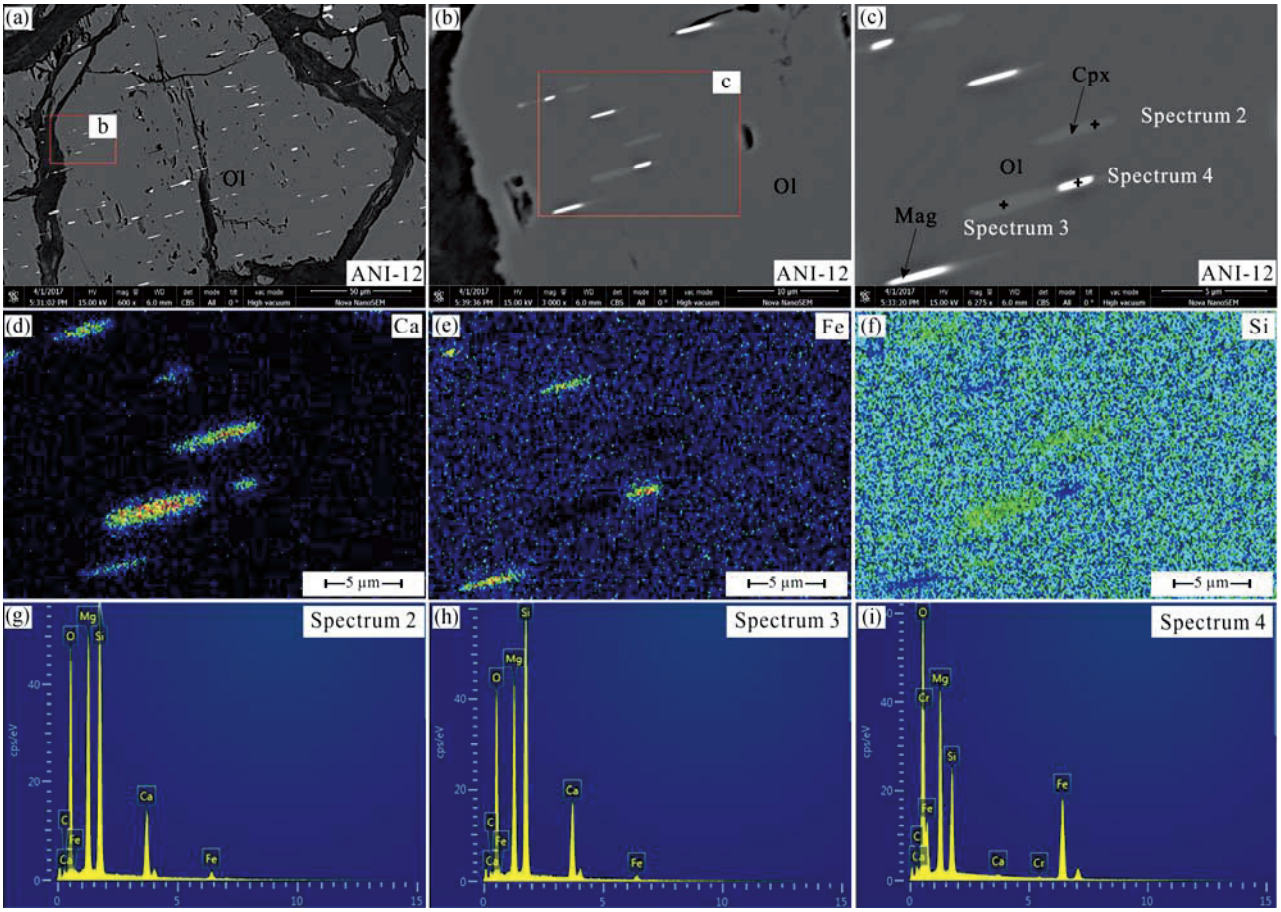

Fig. 7. Backscattered electron images of intergrowth in olivine grains of the Yellow Hill dunite (a–c); Elemental mapping (Ca, Fe and Si) of clinopyroxene lamellae and clinopyroxene-magnetite intergrowth in olivine from the Annette Island dunite (d–f); Energy dispersive spectrometry analysis of clinopyroxene lamellae, clinopyroxene and magnetite intergrowth (g–i).

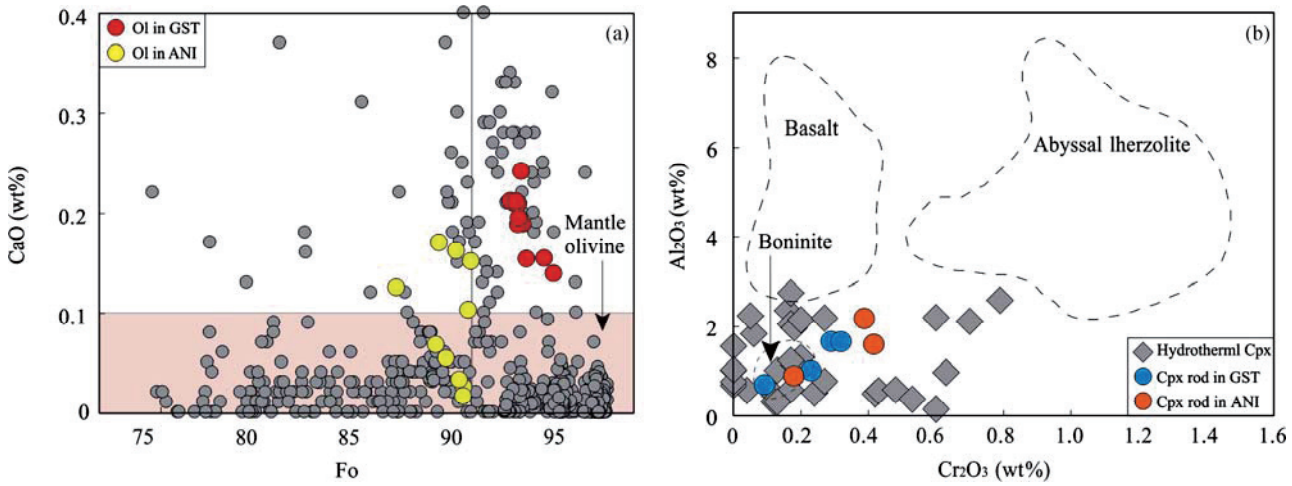

Fig. 8. Correlation diagrams of (a) CaO and Fo in the olivine grains of dunite from the Gaositai and Yellow Hill Alaskan-type complexes and (b) Al_2O_3 and Cr_2O_3 of the clinopyroxene in the intergrowth rod-like features in olivine grain in the dunite from the Gaositai and Yellow Hill Alaskan-type complexes.

Gray circle in Fig. 8a represents the olivine from Alaskan-type complexes worldwide (Bai et al., 2017). The field of mantle olivine in the Fig. 8a is from Bai et al. (2017). Gray diamond in Fig. 8b represents hydrothermal clinopyroxene (Akizawa et al., 2011; Zhang et al., 2016, 2017). Clinopyroxene data in basalt, komatiite, boninite and hydrothermal rocks are from Leterrier et al. (1982), Parman et al. (2003), Bloomer and Hawkins (1987), Sobolev and Danyushevsky (1994) and Akizawa et al. (2011).

Table 2 Temperature and oxygen fugacity of dunite samples from the Gaositai, Yellow Hill Alaskan-type complexes, and Kızıldağ ophiolite

Sample		YH-05	ANI-20	ANI-13	ANI-10	ANI-05	ANI-12	ANI-15	ANI-22	ANI-18	GST-13	GST-15	GST-17	GST-16	GST-31	GST-21	GST-18	GST-33	KZ14-28-2
converted from K	T (°C)	773	692	717	760	762	659	705	730	689	802	773	855	842	846	786	751	660	919
$Fe^2/(Fe^2+Mg)$	XFe-olv	0.11	0.10	0.11	0.14	0.10	0.10	0.12	0.11	0.10	0.07	0.08	0.08	0.06	0.08	0.08	0.07	0.07	0.07
$Mg/(Fe^2+Mg)$	XMg-olv	0.89	0.90	0.89	0.86	0.90	0.90	0.88	0.89	0.90	0.93	0.92	0.92	0.94	0.92	0.92	0.93	0.93	0.93
$Fe^2/(Fe^2+Mg)$	XFe^2-spin	0.64	0.67	0.70	0.75	0.62	0.73	0.72	0.70	0.69	0.53	0.54	0.50	0.45	0.50	0.53	0.55	0.66	0.32
$Mg/(Fe^2+Mg)$	XMg-spin	0.36	0.33	0.30	0.25	0.38	0.27	0.28	0.30	0.31	0.47	0.46	0.50	0.55	0.50	0.47	0.45	0.34	0.68
$Al/sumR^{3+}$	XAl-spin	0.15	0.19	0.17	0.15	0.20	0.19	0.18	0.16	0.23	0.13	0.15	0.14	0.14	0.14	0.15	0.15	0.13	0.28
$Fe^3/sumR^{3+}$	XFe^3-spin	0.19	0.17	0.20	0.34	0.19	0.26	0.25	0.28	0.24	0.17	0.16	0.23	0.19	0.17	0.14	0.15	0.20	0.06
$Cr/sumR^{3+}$	XCr-spin	0.67	0.64	0.63	0.52	0.61	0.55	0.57	0.56	0.53	0.70	0.69	0.63	0.67	0.69	0.71	0.70	0.67	0.66
Ti cations to 4 oxygens	XTi-spin	0.02	0.02	0.02	0.03	0.02	0.02	0.02	0.02	0.02	0.01	0.01	0.01	0.01	0.01	0.01	0.01	0.01	0.01
(XMgolv*XFe^2spin)/ (XFeolv*XMgsp)	KD-MgFe-olvspin	15.1	18.4	17.8	19.0	14.5	23.7	19.6	18.8	18.7	13.7	14.3	12.2	12.0	11.7	13.6	15.3	24.2	6.5
	lnKD	2.71	2.91	2.88	2.94	2.67	3.16	2.98	2.93	2.93	2.62	2.66	2.50	2.49	2.46	2.61	2.73	3.19	1.87
	Log fo_2	−15.3	−17.3	−16.7	−15.6	−15.6	−18.3	−17.0	−16.4	−17.4	−14.7	−15.3	−13.6	−13.9	−13.8	−15.0	−15.8	−18.2	−12.4
	T (K)	1046	965	990	1033	1035	932	978	1003	962	1075	1046	1128	1115	1119	1059	1024	933	1192

Note: Temperature and oxygen fugacity estimated using the olivine-spinel thermometer defined by Ballhaus et al. (1991).

0.21wt%) and FeO (6.63–8.95wt%) contents (Fig. 5a–b; Table 1; Chen et al., 2015). There is no compositional difference between the lamella-bearing and lamella-free olivine grains (Table 1). The equilibrium temperature of the dunite in the Kızıldağ ophiolite is estimated to be 919° C (Table 2).

4.4 Hongshishan mafic-ultramafic complex

Unlike the dunite samples from the above-mentioned three complexes, only chromite needles are observed in olivine grains in one dunite sample from the Hongshishan mafic-ultramafic complex. They are 5 to 10 μm in length and aligned parallel to one another (Fig. 9e, f).

The olivine grains with chromite lamellae in the Hongshishan dunite have compositions similar to the lamella-free olivine grains. They have lower MgO (46.5–47.6wt%) and CaO (0.05–0.06wt%), and higher FeO (11.4–12.6wt%) contents than those in the above-mentioned three complexes (Fig. 5a–b; Table 1; Su Benxun et al., 2009; Su et al., 2012).

5 Discussion

5.1 Exsolved lamellae in olivine grain from previous studies

Exsolved lamellae of ilmenite, chromite and magnetite and intergrowth of chromite/magnetite-silicate have been reported in meteorite, alpine peridotite, layered intrusion and ophiolite (Burns, 1975; Arai, 1978; Ashworth, 1979; Moseley, 1981; Green and Gueguen, 1983; Drury and Van Roermund, 1988; Mikouchi et al., 1995; Zhang et al., 1999; Ren Yufeng et al., 2008; Xiong Fahui et al., 2015, 2016; Xiong et al., 2017). The exsolved ilmenite lamellae in olivine were mostly reported in UHP peridotite (Hacker

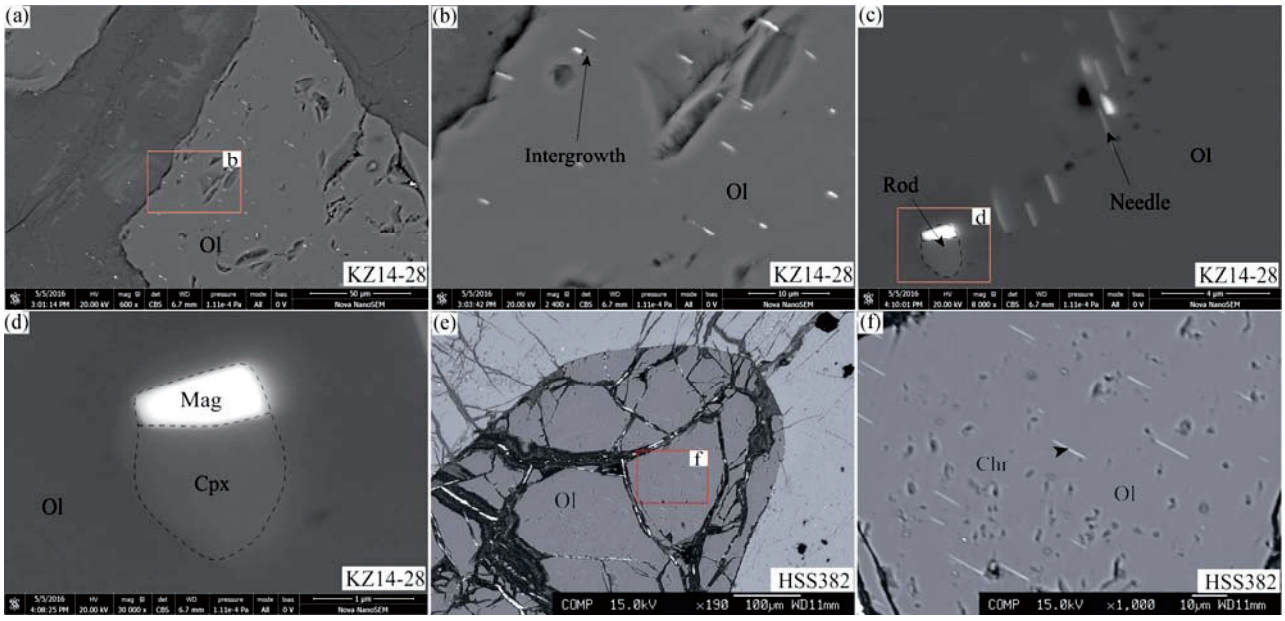

Fig. 9. Backscattered electron images of clinopyroxene-magnetite intergrowth in olivine grains of dunite in the Kızıldağ ophiolite that feature in the absence of occurrence of single clinopyroxene lamellae, the rod- and needle-like intergrowths are oriented in olivine grains (a–d); Backscattered electron images of chromite lamellae in olivine grains form dunite in the Hongshishan complex; the exsolved chromite lamellae are oriented in olivine grains (e–f).

et al., 1997; Jin Zhenmin et al., 1998; Zhang and Liou, 1999; Kadarusman et al., 2000) and are attributed to decomposition of the olivine phase with wadsleyite structure (Zhang and Liou, 1999; Liu Xiangwen et al., 2005).

Exsolved chromite or intergrowth of chromite and diopside in olivine were interpreted as products of the annealing process of olivine solid exsolution initially equilibrating with magnesian Cr-rich liquid. The feasible reaction is as follows (Arai, 1978):

$Cr_{4/3}SiO_4$ (in olivine) + Ca_2SiO_4 (in olivine) + forsterite = chromite + diopside

During the transformation of wadsleyite (α-phase) to olivine, excess Fe_3O_4 component exsolved to form the magnetite lamellae. This type of magnetite commonly occurs as single mineral phase in olivine grains, indicating UHP environment (Hacker et al., 1997; Jin Zhenmin et al., 1998; Zhang and Liou, 1999; Kadarusman et al., 2000). This type of exsolution involved in the phase transformation belongs to the metamorphic exsolution. However, in both natural and experimental samples, the magnetite lamellae are commonly connected with silicates to form intergrowth. This occurrence has been reported as magnetite-orthopyroxene intergrowth in basaltic olivine (Haggerty and Baker, 1967), Precambrian cumulates (Goode, 1974), layered mafic intrusion (Ambler and Ashley, 1977), as magnetite-augite intergrowth in layered intrusions (Moseley, 1984), and as magnetite-diopside intergrowth in a shallow-level mafic intrusion (Ashworth and Chamber, 2000) and ophiolites (Ren Yufeng et al., 2008; Xiong Fahui et al., 2015, 2016; Xiong et al., 2017). The occurrence of magnetite-orthopyroxene intergrowth has been interpreted to result from sub-solidus oxidation of olivine grains with low Fo contents (63–75) (Haggerty and Baker, 1967; Champness, 1970; Goode, 1974; Putnis, 1979; Rietmeijer, 1996). The given reaction is:

$3Mg_2SiO_4 + 3Fe_2SiO_4 + O_2 = 2Fe_3O_4 + 6MgSiO_3$;

The magnetite-augite intergrowth was attributed to the decomposition of Fe^{3+}-bearing, high-T olivine grains during cooling (Moseley, 1984), with a reaction as follows:

$3Fe_{4/3}SiO_4 + Fe_2SiO_4 + 4X_2SiO_4 = 2Fe_3O_4 + 4X_2Si_2O_6$ (where X = Ca, Mg, Fe).

5.2 Origin of clinopyroxene lamellae and clinopyroxene -magnetite intergrowth

As noted above, the oxidation of olivine or decomposition of Fe^{3+}-bearing high-T olivine invariably requires additional orthopyroxene or augite phases associated with magnetite (Haggerty and Baker, 1967; Champness, 1970; Putnis, 1979; Moseley, 1984; Rietmeuer, 1996). The olivine grains of the dunite in the Gaositai and Yellow Hill Alaskan-type complexes and the Kızıldağ ophiolite have high Fo contents ranging from 86.5 to 93.4, and their exsolved intergrowth is dominated by intergrowth of diopside-magnetite (Figs. 3, 6). There is no ilmenite exsolved lamella in the studied olivine. Thus, the occurrence of exsolution in this study can neither be attributed to oxidation of olivine or decomposition Fe^{3+}-olivine during cooling nor be caused by the

metamorphism in the UHP environment.

Normally, olivine accommodates extremely small quantities of Ca^{2+}, Al^{3+} and Na^{+} ions in its crystal lattice due to the larger ionic radii of these elements compared to those of Fe^{2+}, Mg^{2+} and Mn^{2+}. Olivine is thus not expected to exsolve clinopyroxene. Experimental studies of the olivine-melt system show that the higher the contents of CaO, Na_2O and Fe^{2+} in the melt, the higher the Ca content in the olivine. In this study, olivine grains with exsolution microstructures show relatively high CaO contents (especially samples in the Gaositai and Yellow Hill complex; Figs. 5a, 8a). The CaO content in the olivine cannot indicate fractional crystallization, neither could it be affected directly by oxygen fugacity, temperature and pressure (Libourel, 1999). Thus, the variation of CaO content of olivine in the dunite from the Alaskan-type complexes and ophiolites (Figs. 5a, 8a) may be related to later modification of melt/fluid. The rod-like intergrowths in the Gaositai and Yellow Hill olivine grains are aligned in the same direction with the needle-like intergrowths, indicating their simultaneous exsolution. These clinopyroxenes in the rod-like intergrowths mostly fall into the compositional field of hydrothermal clinopyroxene (Fig. 8b). It has been documented that clinopyroxene can crystallize from hydrothermal fluids at temperatures higher than 750°C (Python et al., 2007; Akizawa et al., 2011; Akizawa and Arai, 2014). The anhedral clinopyroxene coexisting with chromite and the presence of interstitial clinopyroxene in the Yellow Hill dunite (Fig. 2e) indicate the involvement of fluids during the formation of the dunite. Hence, the reactant fluids could have originated from hydrothermal fluids.

Re-equilibration between olivine and fluids at high temperatures could produce olivine solid solutions with Ca^{2+}, Si^{4+} and Na^{+} in olivine. The fluids could provide additional Fe^{3+} with olivine. The reaction is as follows:

$2Fe_2^{2+}SiO_4 = 2SiO_2 + Fe^{2+}Fe_2^{3+}O_4 + 2e^{-} + Fe^{2+}$ or: $3Fe_2^{2+}SiO_4 = 3SiO_2 + 2Fe_2^{3+}O_3 + 4e^{-} + 2Fe^{2+}$

This could lead to the extraction of Cr^{3+} and Al^{3+} in the lattice of olivine (Dyar et al., 1998; Ashworth and Chambers, 2000). With decreasing temperature, the olivine solid solution might break down to exsolve magnetite and clinopyroxene. The Fe^{3+} and Cr^{3+} preferentially partition into magnetite, while Ca^{2+} and Na^{+} enter clinopyroxene. Textural and compositional similarities of the diopside-magnetite intergrowth in the olivine grains of dunite in the Luobusa, Dongbo, Purang and Tethyan ophiolites (Ren Yufeng et al., 2008; Xiong Fahui et al., 2015, 2016; Xiong et al., 2017) may also suggest a similar origin of fluids modification.

5.3 Origin of chromite lamellae in olivine grain from Hongshishan dunite

The chromite exsolution lamellae in olivine from the Hongshishan dunite occur in the core of the olivine grains without accompanying silicate material. In previous studies, the exsolution of chromite in olivine was attributed to the pressure-released oxidation of Cr^{2+} initially incorporated in olivine (Burns, 1975) or the annealing process of olivine solid exsolution initially equilibrated with magnesian Cr-rich liquid (Arai, 1978). Accordingly, the exsolved chromite lamellae in the olivine grains from the Hongshishan complex that formed in post-orogenic extension setting may be related to the re-equilibration of olivine with Cr-bearing liquid. In the olivine solid exsolution, Cr^{3+} probably dissolved in the octahedral site of olivine via the following substitution: 3 (Mg, Fe^{2+})=2Cr^{3+}. During the annealing process, Cr^{3+} would enter the exsolved chromite.

5.4 Implications

Clinopyroxene lamellae and clinopyroxene-magnetite intergrowth have been found only in dunite from Alaskan-type complexes and ophiolites (this study; Ren Yufeng et al., 2008; Xiong Fahui et al., 2015, 2016; Xiong et al., 2017). Based on partition coefficients between olivine and pyroxene, Ca^{2+} and Cr^{3+} of the fluids are preferentially incorporated into pyroxene at high temperature, compared to olivine (Bodinier et al., 1987; Libourel, 1999). Thus the exsolution of clinopyroxene and intergrowth occur in dunite and rarely in pyroxene-bearing rocks such as harzburgite and lherzolite.

Alaskan-type complexes are commonly situated at convergent plate margins and subduction-influenced settings (Murray, 1972; Garuti, 2011), and their ultramafic -mafic rocks have been proposed to crystallize from hydrous, high-Mg basaltic magmas (Murray, 1972; Thakurta et al., 2008). Most ophiolite massifs were considered to have initially formed at mid-ocean ridge environments and subsequently modified at supra-subduction zone settings (Lytwyn and Casey, 1993; Dilek and Furnes, 2009; Liu et al., 2014; Li et al., 2015). Dunite in the mantle sequence of ophiolites is normally interpreted as a product of melt-rock interaction where the melt is expected to be sufficiently H_2O-rich (Zhou et al., 1996, 2005). In the studied dunite samples, the H_2O-rich fluids provided additional elements that olivine lacks and therefore, favor serpentinization of the samples. The oxygen fugacity for the studied dunite samples, determined from mineralogy and temperature, indicates that the oxidation state is close to FMQ (Fig. 10). The equilibrium crystalline temperatures are in ranges of 751–855°C for olivine and chromite in the Gaositai complex, 659–773°C in the Yellow Hill complex, and 919°C in the

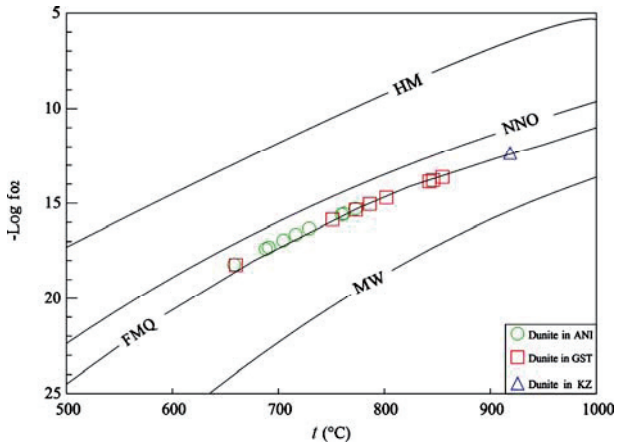

Fig. 10. Correlation diagram of temperature and oxygen fugacity calculated using the thermometer defined by Ballhaud et al. (1991).
Four oxygen reference buffers, namely HM (magnetite-hematite), NNO (Ni-NiO), FMQ (fayalite-magnetite-quartz), and MW (magnetite-wüstite) (Chou, 1978), are plotted for comparison.

Kızıldağ ophiolite, which are higher than the stability temperature of serpentinization (600–650°C), indicating that serpentinization occur during the annealing process of the dunite. Thus, the process of exsolution has genetic relationship with serpentinization.

6 Conclusions

Exsolution microstructures in clinopyroxene and clinopyroxene-magnetite intergrowth in the Gaositai and Yellow Hill Alaskan-type complexes, clinopyroxene-magnetite intergrowth in the Kızıldağ ophiolite, and chromite lamellae from the Hongshishan mafic-ultramafic complex commonly occur as needle-like or rod-like features in olivine grains. The chemical compositions of the clinopyroxene in the rod-like intergrowth indicate that its origin is probably related with reaction between dunite and fluids. Since the formation of both Alaskan-type complex and ophiolites are related to subduction environment, the fluids could be released from the subducted slab. In contrast, the exsolved chromite lamellae in olivine grains from the Hongshishan complex that formed in post-orogenic extension setting can be related to re-equilibration of olivine with Cr-bearing liquid. Similarly, the clinopyroxene lamellae and clinopyroxene-magnetite intergrowth show spatial relations with serpentinization occurring in the dunite, indicating possible genetic relations with serpentinization.

Acknowledgements

We would like to thank Di Zhang, Saihong Yang and Wenqiang Yang for their assistance with the chemical analyses. We thank three anonymous reviewers for their constructive and detailed comments and the editor for editorial handling of this manuscript. This study was financially supported by the National Natural Science Foundation of China (Grants 41522203, 41673037 and 41772055) and Youth Innovation Promotion Association, Chinese Academy of Sciences (Grant 2017095).

Manuscript received Sept. 15, 2017
accepted Nov. 30, 2017
edited by Fei Hongcai

References

Agee, C.B., and Walker, D., 1990. Aluminum partitioning between olivine and ultrabasic silicate liquid to 6 GPa. *Contributions to Mineralogy and Petrology*, 105: 243–254.

Akizawa, N., Arai, S., Tamura, A., Uesugi, J., and Python, M., 2011. Crustal diopsidites from the northern Oman ophiolite: evidence for hydrothermal circulation through suboceanic Moho. *Journal of Mineralogical and Petrological Sciences*, 106: 261–266.

Akizawa, N., and Arai, S., 2014. Petrology of mantle diopsidite from Wadi Fizh, northern Oman ophiolite: Cr and REE mobility by hydrothermal solution. *Island Arc*, 23: 312–323.

Ambler, E.P., and Ashley, P.M., 1977. Vermicular orthopyroxene-magnetite symplectites from the Wateranga layered mafic intrusion, Queensland, Australia. *Lithos*, 10: 163–172.

Aoki, K.I., Fujimaki, H., and Kitamura, M., 1980. Exsolved garnet-bearing pyroxene megacrysts from some South African kimberlites. *Lithos*, 13: 269–279.

Arai, S., 1978. Chromian spinel lamellae in olivine from the Iwanai-dake peridotite mass, Hokkaido, Japan. *Earth and Planetary Science Letters*, 39: 267–273.

Ashworth, J.R., 1979. Two kinds of exsolution in chondritic olivine. *Mineralogical Magazine*, 43: 535–538.

Ashworth, J.R., and Chambers, A.D., 2000. Symplectic reaction in olivine and the controls of intergrowth spacing in symplectites. *Journal of Petrology*, 41: 285–304.

Ballhaus, C., Berry, R.F., and Green, D.H., 1991. High pressure experiment calibration of the olivine-orthopyroxene-spinel oxygen geobarmeter: implications for the oxidation state of the upper mantle. *Contributions to Mineralogy and Petrology*, 107: 27–40.

Bai, Y., Su, B.X., Chen, C., Yang, S.H., Liang, Z., Xiao, Y., Qin, K.Z., and Malaviarachchi, S.P.K., 2017. Base metal mineral segregation and Fe-Mg exchange inducing extreme compositions of olivine and chromite from the Xiadong Alaskan-type complex in the southern part of the Central Asian Orogenic Belt. *Ore Geology Reviews*, 90: 184–192.

Bloomer, S.H., and Hawkins, J.W., 1987. Petrology and geochemistry of boninite series volcanic rocks from the Mariana trench. *Contributions to Mineralogy and Petrology*, 97: 361–377.

Bodinier, J.L., Dupuy, C., and Dostal, J., 1987. Distribution of trace transition elements in olivine and pyroxenes from ultramafic xenoliths: Application of microprobe analysis. *American Mineralogist*, 72: 902–913.

Boulton, S.J., and Robertson, A.H.F., 2007. The Miocene of the

Hatay area, S Turkey: Transition from the Arabian passive margin to an underfilled foreland basin related to closure of the Southern Neotethys Ocean. *Sedimentary Geology*, 198: 93–124.

Bozhilov, K.N., Green, H.W., and Dobrzhinetskaya, L., 1999. Clinoenstatite in Alpe Arami peridotite: additional evidence of very high pressure. *Science*, 284: 128–132.

Burns, R.G., 1975. Crystal field effects in chromium and its partitioning in the mantle. *Geochimica et Cosmochimica Acta*, 39: 857-864.

Champness, P.E., 1970. Nucleation and growth of iron oxides in olivines, $(Mg, Fe)_2SiO_4$. *Mineralogical Magazine*, 37: 790–800.

Chen, B., Suzuki, K., Tian, W., Jahn, B.M., and Ireland, T., 2009. Geochemistry and Os-Nd-Sr isotopes of the Gaositai Alaskan-type ultramafic complex from the northern North China craton: implications for mantle-crust interaction. *Contributions to Mineralogy and Petrology*, 158: 683–702.

Chen, C., Su, B.X., Uysal, I., Avci, E., Zhang, P.F., Xiao, Y., and He, Y.S., 2015. Iron isotopic constraints on the origin of peridotite and chromitite in the Kızıldağ ophiolite, southern Turkey. *Chemical Geology*, 417: 115–124.

Chou, I.M., 1978. Calibration of oxygen buffers at elevated P and T using the hydrogen fugacity sensor. *American Mineralogist*, 63: 690–703.

Clarke, D.B., and Pe-Piper, G.G., 1983. Multiply exsolved clinopyroxene megacrysts from the Frank Smith mine, Cape Province, South Africa. *Lithos*, 16: 75–84.

Colás, V., Padrón-Navarta, J.A., González-Jiménez, J.M., Griffin, W.L., Fanlo, I., O'Reilly, S.Y., Gervilla, F., Proenza, J.A., Pearson, N.J., and Escayola, M.P., 2016. Compositional effects on the solubility of minor and trace elements in oxide spinel minerals: insights from crystal-crystal partition coefficients in chromite exsolution. *American Mineralogist*, 101: 1360–1372.

Dilek, Y., and Furnes, H., 2009. Structure and geochemistry of Tethyan ophiolites and their petrogenesis in subduction rollback systems. *Lithos*, 113: 1–20.

Dilek, Y., and Thy, P., 2009. Island arc tholeiite to boninitic melt evolution of the Cretaceous Kızıldağ (Turkey) ophiolite: Model for multi-stage early arc-forearc magmatism in Tethyan subduction factories. *Lithos*, 113: 68–87.

Dilek, Y., and Furnes, H., 2017. Geochemical characterization of intermediate to silicic rocks in the global ophiolites record. *Acta Geologica Sinica* (English edition), 91(z1): 8–9.

Dodd, R.T., 1973. Minor element abundances in olivines of the Sharps (H-3) chondrite. *Contributions to Mineralogy and Petrology*, 42: 159–167.

Drury, M.R., and Van Roermund, H.L.M., 1988. Metasomatic origin for Fe-Ti-rich multiphase inclusions in olivine from kimberlite xenoliths. *Geology*, 16: 1035–1038.

Dyar, M.D., Delaney, J.S., Sutton, S.R., and Schaefer, M.W., 1998. Fe^{3+} distribution in oxidized olivine: A synchrotron micro-XANES study. *American Mineralogist*, 83: 1361–1365.

Garuti, G., 2011. Global tectonics and chromite-platinum mineralization monitoring genesis and evolution of Ural-Alaskan-type complexes. *Revista Macla*, 15: 15–16.

Gehrels, G.E., Saleeby, J.B., and Berg, H.C., 1987. Geology of Annette, Gravina, and Duke islands, southeastern Alaska. *Canadian Journal of the Earth Sciences*, 24: 866–881.

Goode, A.D.T., 1974. Oxidation of natural olivines. *Nature*, 248: 500–501.

Green, D.H., 1966. The origin of the "eclogites" from Salt Lake Crater, Hawaii. *Earth and Planetary Science Letters*, 1: 414–420.

Green, H.W., and Gueguen, Y., 1983. Deformation of peridotite in the mantle and extraction by kimberlite: a case history documented by fluid and solid precipitates in olivine. *Tectonophysics*, 92: 71–92.

Grove, T.L., Till, C.B., and Krawczynski, M.J., 2012. The role of H_2O in subduction zone magmatism. *Annual Review of Earth and Planetary Sciences*, 40: 413–439.

Hacker, B.R., Sharp, T., Zhang, R.Y., Liou, J.G., and Hervig, R.L., 1997. Determining the origin of ultrahigh-pressure lherzolites. *Science*, 278: 702–707.

Haggerty, S.E., and Baker, L., 1967. The alteration of olivine in basaltic and associated lavas. *Contributions to Mineralogy and Petrology*, 16: 233–257.

Hall, R., 1976. Ophiolite emplacement and the evolution of the Taurus suture zone, southeastern Turkey. *Geological Society of America Bulletin*, 87: 1078–1088.

Hess, H.H., 1960. Stillwater igneous complex, Montana a quantitative mineralogical study. *Geological Society of America Memoirs*, 80: 1–240.

Jerde, E.A., Taylor, L.A., Crozaz, G., and Sobolev, N.V., 1993. Exsolution of garnet within clinopyroxene of mantle eclogites: major and trace-element chemistry. *Contributions to Mineralogy and Petrology*, 114: 148–159.

Jin Zhenmin, Jin Shuyan, Gao Shan and Zhao Wenxia, 1998. Is the depth of formation of ultrahigh-P rock from the Dabie Mountains limited to 100-150 km? : Discovery of Ti-Cr magnetite needle and its significance for dynamics. *Chinese Science Bulletin*, 43: 767–771 (in Chinese).

Kadarusman, A., and Parkinson, C.D., 2000. Petrology and P-T evolution of garnet peridotites from central Sulawesi, Indonesia. *Journal of Metamorphic Geology*, 18: 193–210.

Kerrich, R., and Polat, A., 2006. Archean greenstone-tonalite duality: thermochemical mantle convection models or plate tectonics in the early Earth global dynamics? *Tectonophysics*, 415: 141–165.

Kirby, S.H., and Etheridge, M.A., 1981. Exsolution of Ca-clinopyroxene from orthopyroxene aided by deformation. *Physics and Chemistry of Minerals*, 7: 105–109.

Lappin, M.A., and Dawson, J.B., 1975. Two Roberts Victor cumulate eclogites and their re-equilibration. *Physics and Chemistry of the Earth*, 9: 351–365.

Leterrier, J., Maury, R.C., Thonon, P., Girard, D., and Marchal, M., 1982. Clinopyroxene composition as a method of identification of the magmatic affinities of paleo-volcanic series. *Earth and Planetary Science Letter*, 59: 139–154.

Li, C., Ripley, E.M., Thakurta, J., Stifter, E.C., and Qi, L., 2013. Variations of olivine Fo-Ni contents and highly chalcophile element abundances in arc ultramafic cumulates, southern Alaska. *Chemical Geology*, 351: 15–28.

Li, X.P., Chen, H.K., Wang, Z.L., Wang, L.J., Yang, J.S., and Robinson, P., 2015. Spinel peridotite, olivine websterite and the textural evolution of the Purang ophiolite complex, western Tibet. *Journal of Asian Earth Sciences*, 110: 55–71.

Libourel, G., 1999. Systematics of calcium partitioning between olivine and silicate melt: implications for melt structure and calcium content of magmatic olivines. *Contributions to Mineralogy and Petrology*, 136: 63–80.

Liu, C.Z., Zhang, C., Yang, L.Y., Zhang, L.L., Ji, W.Q., and Wu, F.Y., 2014. Formation of gabbronorites in the Purang ophiolite (SW Tibet) through melting of hydrothermally altered mantle along a detachment fault. *Lithos*, 205: 127–141.

Liu Xiangwen, Jin Zhenmin, Qu Jing and Wang Lu, 2005. Exsolution of ilmenite and Cr-Ti magnetite from olivine of garnet-wehrlite. *Science in China Series D: Earth Sciences*, 48: 1368–1376 (in Chinese).

Lytwyn, J.N., and Casey, J.F., 1993. The geochemistry and petrogenesis of volcanic and sheeted dikes from the Hatay (Kızıldağ) ophiolite, southern Turkey: possible formation with the Troodos ophiolite, Cyprus, along fore-arc spreading centers. *Tectonophysics*, 223: 237–272.

Matveev, S., and Ballhaus, C., 2002. Role of water in the origin of podiform chromitite deposits. *Earth and Planetary Science Letters*, 203: 235–243.

Mikouchi, T., Takeda, H., and Miyamoto, M., 1995. Exsolution lamellae of kirschsteinite in magnesium-iron olivine from an angrite meteorite. *American Mineralogist*, 80: 585–592.

Moseley, D., 1981. Ilmenite exsolution in olivine. *American Mineralogist*, 66: 976–979.

Moseley, D., 1984. Symplectic exsolution in olivine. *American Mineralogist*, 69: 139–153.

Murray, C.G., 1972. Zoned ultramafic complexes of the Alaskan type: feeder pipes of andesitic volcanoes. *Geological Society of America Memoir*, 132: 313–335.

Parman, S.W., Shimizu, N., Grove, T.L., and Dann, J.C., 2003. Constraints on the pre-metamorphic trace element composition of Barberton komatiites from ion probe analyses of preserved clinopyroxene. *Contributions to Mineralogy and Petrology*, 144: 383–396.

Putnis, A., 1979. Electron petrography of high-temperature oxidation in olivine from the Rhum layered intrusion. *Mineralogical Magazine*, 43: 293–296.

Python, M., Ishida, Y., Ceuleneer, G., and Arai, S., 2007. Trace element heterogeneity in hydrothermal diopside: evidence for Ti depletion and Sr-Eu-LREE enrichment during hydrothermal metamorphism of mantle harzburgite. *Journal of Mineralogical and Petrological Sciences*, 102: 143–149.

Reiche, M., and Bautsch, H.J., 1985. Electron microscopical study of garnet exsolution in orthopyroxene. *Physics and Chemistry of Minerals*, 12: 29–33.

Ren Yufeng, Chen Fangyuan, Yang Jingsui and Gao Yuanhong, 2008. Exsolutions of diopside and magnetite in olivine from mantle dunite, Luobusa ophiolite, Tibet, China. *Acta Geologica Sinica* (English edition), 82(2): 377–384.

Rietmeijer, F.J.M., 1996. Cellular precipitates of iron oxide in olivine in a stratospheric interplanetary dust particle. *Mineralogical Magazine*, 60: 877–885.

Sautter, V., and Harte, B., 1988. Diffusion gradients in an eclogite xenolith from the Roberts Victor kimberlite pipe: 1. Mechanism and evolution of garnet exsolution in Al_2O_3-rich clinopyroxene. *Journal of Petrology*, 29: 1325–1352.

Sautter, V., and Hart, B., 1990. Diffusion gradients in an eclogite xenolith from the Roberts Victor kimberlite pipe: kinetics and implications for petrogenesis. *Contributions to the Mineralogy and Petrology*, 105: 637–649.

Schmickler, B., Jacob, D.E., and Foley, S.F., 2004. Eclogite xenoliths from the Kuruman kimberlites, South Africa: geochemical fingerprinting of deep subduction and cumulate processes. *Lithos*, 75: 173–207.

Sobolev, A.V., and Danyushevsky, L.V., 1994. Petrology and geochemistry of boninites from the north termination of the Tonga Trench: constraints on the generation conditions of primary high-Ca boninite magmas. *Journal of Petrology*, 35: 1183–1211.

Spandler, C., O'Neill, H.S.C., and Kamenetsky, V.S., 2007. Survival times of anomalous melt inclusions from element diffusion in olivine and chromite. *Nature*, 447: 303–306.

Su Benxun, Qin Kezhang, Sun He, Tang Dongmei, Xiao Qinghua and Cao Mingjian, 2009. Petrological and mineralogical characteristics of Hongshishan mafic-ultramafic complex in Beishan area, Xinjiang: Implications for assimilation and fractional crystallization. *Acta Petrologica Sinica*, 25: 873–887 (in Chinese with English abstract).

Su, B.X., Qin, K.Z., Sakyi, P.A., Tang, D.M., Liu, P.P., Malaviarachchi, S.P.K., Xiao, Q.H., and Sun, H., 2012. Geochronologic-petrochemical studies of the Hongshishan mafic-ultramafic intrusion, Beishan area, Xinjiang (NW China): petrogenesis and tectonic implications. *International Geology Review*, 54: 270–289.

Thakurta, J., Ripley, E.M., and Li, C., 2008. Geochemical constraints on the origin of sulfide mineralization in the Duke Island Complex, southeastern Alaska. *Geochemistry Geophysics Geosystem*, 9: 3562–3585.

Tian, W., Chen, B., Ireland, T.R., Green, D.H., Suzuki, K., and Chu, Z., 2011. Petrology and geochemistry of dunites, chromitites and mineral inclusions from the Gaositai Alaskan-type complex, North China Craton: Implications for mantle source characteristics. *Lithos*, 127: 165–175.

Xiong Fahui, Yang Jingsui, Robinson, P.T., Dilek, Y., Chen Yanhong, Xu Xiangzhen, Liu Zhao, Tian Yazhou, Zhou Wenda, Lai Shengmin and Zhang Lan, 2015. Diopside and magnetite exsolutions in olivine from lower $Cr^{\#}$ dunite in the Dongbo ophiolites, southern Tibet. *Acta Geologica Sinica* (English edition), 89(z2): 101.

Xiong Fahui, Yang Jingsui, Guo Guolin, Liu Zhao, Xu Xiangzhen, Tian Yazhou, Lai Shengmin, Chen Yanhong and Zhang Lan, 2016. Exsolution in olivine from the lower $Cr^{\#}$ dunite in the Purang ophiolite, the western portion of the Yarlung-Zangbo Suture Zone in Tibet. *Acta Geoscientica Sinica*, 37: 79–89 (in Chinese with English abstract).

Xiong, F.H., Yang, J.S., Dilek, Y., and Wang, C.L., 2017. Nanoscale diopside and spinel exsolution in olivine from dunite of the Tethyan ophiolites, southwestern Turkey: implications for the multi-stage process. *Journal of Nanoscience and Nanotechnology*, 17: 6587–6596.

Yamamoto, S., Komiya T., Hirose, K., and Maruyama, S., 2009. Coesite and clinopyroxene exsolution lamellae in chromites: In-situ ultrahigh-pressure evidence from podiform chromitites in the Luobusa ophiolite, southern Tibet. *Lithos*, 109: 314–322.

Zhang, P.F., Uysal, I., Zhou, M.F., Su, B.X., and Avci, E., 2016. Subduction initiation for the formation of high-Cr chromitites in the Kop ophiolite, NE Turkey. *Lithos*, 260: 345–355.

Zhang Pengfei, Zhou Meifu, Su Benxun, Uysal, I., Robinson, P.T., Avci, E., and He Yongsheng, 2017. Iron isotopic fractionation and origin of chromitites in the Paleo-Moho transition zone of the Kop ophiolite, NE Turkey. *Acta Geologica Sinica* (English edition), 91(z1): 53.

Zhang, R.Y., and Liou, J.G., 1999. Exsolution lamellae in minerals from ultrahigh-pressure rocks. *International Geology*

Review, 41: 981–993.

Zhang, R.Y., Shu, J.F., Mao, H.K., and Liou, J.G., 1999. Magnetite lamellae in olivine and clinohumite from Dabie UHP ultramafic rocks, central China. *American Mineralogist*, 84: 564–569.

Zhang, R.Y., and Liou, J.G., 2003. Clinopyroxenite from the Sulu ultrahigh-pressure terrane, eastern China: Origin and evolution of garnet exsolution in clinopyroxene. *American Mineralogist*, 88: 1591–1600.

Zhang, R.Y., Shau, Y.H., Yang, J.S., and Liou, J.G., 2017. Discovery of clinoenstatite in the Luobusa ophiolitic mantle peridotite recovered from a drill hole, Tibet. *Journal of Asian Earth Sciences*, 145: 605–612.

Zhao Wenxia, Hu Yuxian, Xia Feng, Wang Ximei, Liao Chengzhu and Jiang Dan, 2004. K-rich lamellar exsolution in clinopyroxene: Constraint on the depth of peridotite source at Zhimafang. *Chinese Science Bulletin*, 49: 711–715.

Zhou, M.F., Robinson, P.T., Malpas, J., and Li, Z., 1996. Podiform chromitites in the Luobusa ophiolite (southern Tibet): Implications for melt-rock interaction and chromitite segregation in the upper mantle. *Journal of Petrology*, 37: 3–22.

Zhou, M.F., Robinson, P. T., Malpas, J., Edwards, S.J., and Qi, L., 2005. REE and PGE geochemical constraints on the formation of dunites in the Luobusa ophiolite, Southern Tibet. *Journal of Petrology*, 46: 615–639.

Zhu, Y., 2003. Comments on "Crystal-melt equilibria involving potassium-bearing clinopyroxene as indicator of mantle-derived ultrahigh-potassic liquids: an analytical review": by Perchuk, L.L., Safonov, O.G., Yapaskurt, V.O., Barton, J.M., 2002. (Lithos 60, 89–111): K-feldspar in metamorphic clinopyroxene, from exsolution to potassium replacement. *Lithos*, 68: 115–119.

Zhu, Y., and Ogasawara, Y., 2002. Phlogopite and coesite exsolution from super-silicic clinopyroxene. *International Geology Review*, 44: 831–836.

About the first author

LIANG Zi, female, born in 1993 in Xuzhou, Jiangsu Province; a master student of Institute of Geology and Geophysics, Chinese Academy of Sciences; She is now interested in the study on geochemistry of mafic-ultramafic complexes. E-mail: liangzi@mail.iggcas.ac.cn; Phone: 15010010960.